3 September 1976, Volume 193, Number 4256 SCIENCE

X-rays from Coalescing Atoms

X-ray continua from collisions of combined atomic number up to 164 have been detected.

Walter E. Meyerhof

In a collision of two atoms with atomic numbers Z_1 and Z_2, the nuclei may approach each other so closely that, for a very short time, the atomic electrons arrange themselves as if they belonged to a united atom (UA) of atomic number $Z_{UA} = Z_1 + Z_2$. In recent years several interesting applications of these quasiatoms or, more accurately, quasimolecules, have been proposed. First, if $Z_1 + Z_2$ is sufficiently large, such quasimolecules provide a "laboratory" in which the behavior of electrons in the presence of extremely high electric and magnetic fields can be studied (*1, 2*). In particular, the emission of positrons in very energetic collisions between very heavy ions and atoms has been predicted. Possible new tests of quantum electrodynamics under high-field conditions are thereby provided, which, because of the instability of nuclei with $Z \gtrsim 106$, would otherwise be impossible. Second, x-ray emission spectra from quasimolecules may permit spectroscopic studies of superheavy atomic systems with Z_{UA} as high as 184 (*3–6*). Third, the shape and anisotropy of x-ray emission spectra give insight into details of the atomic collision process, such as dependence of the electronic energies on internuclear separation, transition mechanisms and transition probabilities between electronic states, and dynamic line-broadening effects. The intensities of the x-ray spectra, and to some extent their shapes, are related to the production of inner-shell vacancies in atomic collisions. To date, only the second and third of these proposals have been pursued experimentally, and these are the topic of this review.

The entire field has been stimulated through the discovery by Saris *et al.* (*7*) of a quasimolecular x-ray band emitted in Ar + Ar collisions (*8–10*). Meanwhile many such x-ray bands have been observed; three sample spectra are given in Fig. 1.

It is convenient to classify the bands by the UA shell, K, L, or M, to which the electronic transitions between the molecular orbital (MO) levels lead (*3–5, 7, 8, 11*). This article attempts to give an overview of the present state of the field: the evidence for MO x-rays, their properties, and their suggested future uses. It is helpful to examine first the known mechanisms of inner-shell vacancy formation, since they are closely related to MO x-ray production. Possible background continuum spectra have to be considered. Experimental continuum x-ray spectra can then be compared with theoretical models for MO x-ray production (so far this has been done only for K MO x-rays). Finer details of the collisions, some of which are not yet understood, appear in the anisotropy of the spectra with respect to the incident projectile and in studies of x-ray continuum spectra in coincidence with scattered projectiles.

The author is professor and chairman of the Department of Physics, Stanford University, Stanford, California 94305.

Inner-Shell Vacancy Formation

Two extreme models have been proposed for the formation of vacancies in the inner shells of the colliding atoms, which result in the emission of characteristic x-rays or Auger electrons of the separated atoms (SA) (*12*). For brevity these models will be called atomic and molecular, respectively.

In the atomic model one assumes that the Coulomb field of the projectile (Z_1) interacts with a given electron in the target (Z_2). The time variation of the field causes momentum to be transferred to the electron, which is thereby ejected from the target. The electronic structure of the projectile is not taken into account. The initial wave function of the target electron is assumed to be the atomic wave function, undistorted by the projectile. Different variations of this basic model have successfully explained SA vacancy production by collisions in which $Z_1 \ll Z_2$ (*12*).

In the molecular model (*12, 13*) it is assumed that the collision is slow enough that at each internuclear separation R the electronic wave functions in the projectile and the target atoms adjust themselves to the molecular configuration appropriate to a diatomic molecule with nuclear charges Z_1 and Z_2 and internuclear separation R. In this case, the time-varying nature of the projectile and target Coulomb fields at the position of the electron can cause the electron to make transitions to unfilled quasimolecular levels or to the continuum. This allows vacancies to appear in one of the collision partners after the collision. The expenditure of energy in the transition determines the transition probability in a critical way. If the relevant energy levels happen to cross at a given R, or approach each other very closely, there is no expenditure of energy in the transition, and the vacancy production cross section can be very large. If there is an energy gap between the relevant levels, such as is the case in ionization, the cross section can be many orders of magnitude smaller. The molecular model has been very successfully applied to SA vacancy formation in collisions in which

$0.3Z_2 \lesssim Z_1 \lesssim 3Z_2$ and $v_1 \lesssim 0.3\, v_e$, where v_1 is the projectile velocity and v_e the orbital velocity of the "jumping" electron

$$v_e = (2U_e/m)^{1/2} \quad (1)$$

Here U_e is the ionization energy of the initial state and m is the mass of the electron.

Since the preceding conditions on Z_1, Z_2, and v_1/v_e are also those which make possible the observation of MO x-ray bands (Fig. 1), further details of the molecular model are discussed below. It should be noted, though, that as Z_1/Z_2 decreases to small values, there must be a continuous transition from the molecular model to the atomic model. Indeed, using the theory of perturbed stationary states, Basbas, Brandt, and co-workers (*14*) have shown that for $Z_1 \ll Z_2$ the molecular model reduces to a modified atomic model. The modifications reflect the increase in the binding energy of the target electron due to the penetrating projectile (a "molecular" effect) and the Coulomb deflection of the projectile by the target.

Production of Molecular Orbital X-rays

In the molecular model approach, the production of SA and MO x-rays in heavy-ion collisions is best discussed with the aid of correlation diagrams (*12, 13*) such as those shown in Fig. 2. These diagrams are based on the assumption that inner-shell electrons can be treated as independent particles moving in a screened two-center Coulomb field (*5, 15*). This is in contrast to the situation for outer-shell electrons, where multielectron states play a decisive role (*16*). The correlation diagrams show how electrons move from the SA levels to the UA levels by way of the MO levels, as the internuclear separation R changes from infinity to zero. In a collision with an impact parameter b, the projectile moves in an approximately hyperbolic trajectory so that the minimum value of R is (*17*)

$$R_{min} = D/2 + [(D/2)^2 + b^2]^{1/2} \quad (2)$$

Here D is the distance of closest approach in a head-on collision ($b = 0$)

$$D = 2Z_1Z_2e^2/(M_0v_1^2) \quad (3)$$
$$M_0 = M_1M_2/(M_1 + M_2)$$

where e is the electronic charge, and M_1 and M_2 are the projectile and target masses, respectively. Correspondingly, in a collision an electron moves on a correlation diagram from $R = \infty$ to R_{min} and back to $R = \infty$. If, during the collision, the electron makes a transition out of a particular MO level, the vacancy in that level can be filled in the remaining part of the collision with the emission of an MO x-ray, or after the collision with the emission of an SA ("characteristic") x-ray. (Auger electrons can also be emitted.) The probability for emission of an MO x-ray during collision is roughly equal to the ratio of the collision time t_{coll} to the vacancy lifetime τ. For K MO x-ray emission, $t_{coll} \approx a_K/v_1$, where a_K is the UA Bohr K radius and τ can be estimated from the expression (*18*)

$$1/\tau_K = 2.6 \times 10^9 Z^{3.93}\ \text{sec}^{-1} \quad (4)$$

where Z is the UA atomic number. The ratio t_{coll}/τ_K is always very small compared to unity. For example, for Br + Br collisions with a projectile energy of 30 Mev (million electron volts), $t_{coll}/\tau_K \approx 10^{-3}$. Hence, most K MO vacancies terminate with the emission of SA x-rays or Auger electrons.

Cross Sections for K Molecular Orbital X-rays

Contrary to the SA x-rays, which appear as sharp lines in an x-ray spectrum, MO x-rays are expected to form bands. This is because MO x-ray emission can occur at any value of R and the energy separation between MO levels generally varies rapidly as a function of R, usually reaching a maximum at $R = 0$ (see Fig. 2c). This is called the UA limit. Unfortunately, as the preceding estimate shows, the intensity of the MO x-ray bands is weak, so that the bands could be confused with other x-ray continua such as electron or nuclear bremsstrahlung, discussed below (*19*). Therefore, it is important to make absolute predictions of the expected intensities and shapes of MO x-ray spectra for a variety of collision systems and to check whether the experimental spectra agree. So far, this has been done only for K MO x-rays, because here the situation is simplest (*20–23*). Even so, one has to distinguish two separate processes of MO x-ray production.

Referring to Fig. 2, a and b, one can see that K MO x-ray emission requires a prior vacancy in the $1s\sigma$ MO. It is possible that such a vacancy is produced early in a collision and that later in the same collision an MO x-ray is emitted (*20*). This is called the one-collision process. But it is also possible for an (atomic) K vacancy to be produced in the

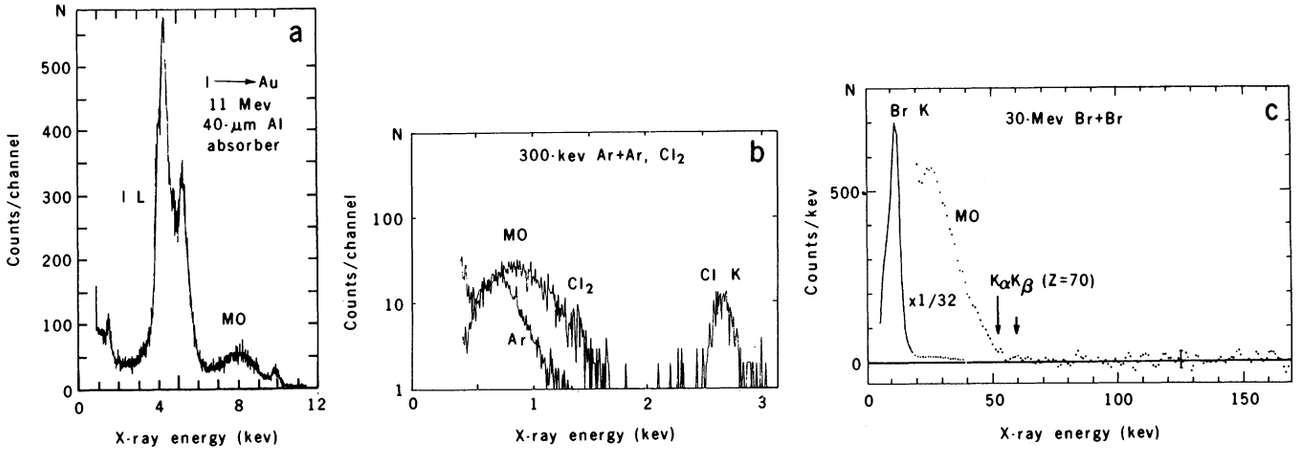

Fig. 1. X-ray spectra from heavy-ion collisions. (a) Spectrum for 11-Mev I + Au. The M MO x-ray band is indicated, as well as the composite L x-ray structure from I. The peak near 10 kev is due to $L\alpha$ x-rays from Au. [From Mokler *et al.* (*4*)] (b) Spectra for 300-kev Ar + Ar and Ar + Cl_2. The L MO x-ray bands are shown, as well as the Cl K peak. [From Hoogkamer *et al.* (*9*)] (c) Spectra for 30-Mev Br + Br. The K MO x-ray band and $Z = 70$ UA $K\alpha$ and $K\beta$ limits are indicated, as well as the Br K x-ray peak. [From Meyerhof *et al.* (*20*)] In (b) and (c) the low-energy portions of the spectra are considerably distorted by absorption effects.

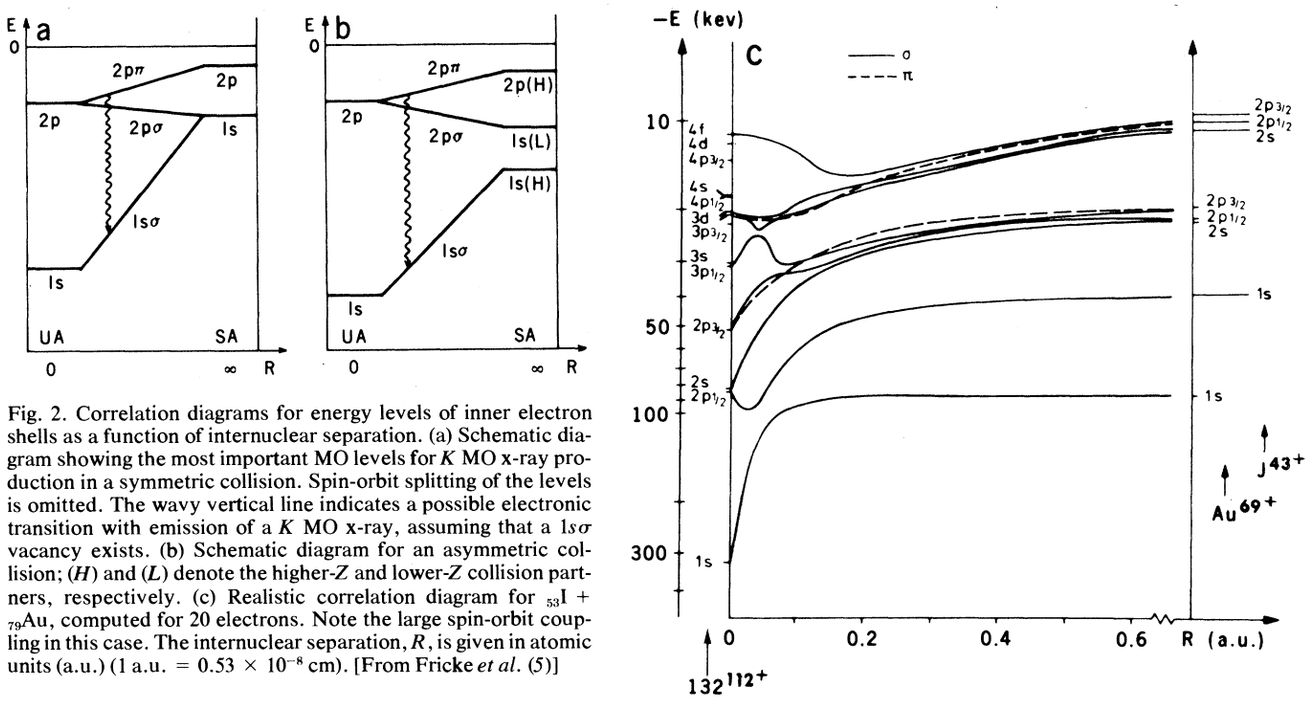

Fig. 2. Correlation diagrams for energy levels of inner electron shells as a function of internuclear separation. (a) Schematic diagram showing the most important MO levels for K MO x-ray production in a symmetric collision. Spin-orbit splitting of the levels is omitted. The wavy vertical line indicates a possible electronic transition with emission of a K MO x-ray, assuming that a $1s\sigma$ vacancy exists. (b) Schematic diagram for an asymmetric collision; (H) and (L) denote the higher-Z and lower-Z collision partners, respectively. (c) Realistic correlation diagram for $_{53}$I + $_{79}$Au, computed for 20 electrons. Note the large spin-orbit coupling in this case. The internuclear separation, R, is given in atomic units (a.u.) (1 a.u. = 0.53×10^{-8} cm). [From Fricke *et al.* (5)]

projectile in a collision and, if the vacancy lives sufficiently long, to be carried into a subsequent collision (*7, 8*). This is called the two-collision process. If the latter collision is symmetric (Fig. 2a), there is a 50 percent probability for the vacancy to move into the $1s\sigma$ MO. It can then be radiatively filled. In an asymmetric collision (Fig. 2b) the situation is more complicated. Either the projectile must be the higher-Z (H) collision partner so that the vacancy is brought into the $1s$(H) state in the second collision or, if the vacancy is brought into the $1s$(L) state, it must jump to the $1s\sigma$ MO early in the second collision. [Such a jumping process does exist (*24*).] Because of the energy gaps involved in creating the $1s$(H) vacancy in the projectile or in the $1s$(L) $\rightarrow$ $1s\sigma$ jumping process, the intensity of the two-collision process diminishes rapidly with increasing asymmetry of the collision (*20*).

One-collision process. The cross section for a one-collision process can be written down readily in the quasistatic approximation. Here one assumes that, once the $1s\sigma$ vacancy has been created, at each internuclear distance R there is a probability $dt/\tau_x(R)$ for the vacancy to be radiatively filled, where $\tau_x(R)$ is the radiative lifetime of the vacancy and dt is an interval of time. Neglecting any coherence or interference effects, the differential cross section for emission of a K MO x-ray with an energy E_x in a collision with impact parameter b is

$$d^2\sigma^{(1)}/dE_x = 2\pi bdb\, P(b)\, (dR/dE_x)/v_R\tau_x(R) \quad (5)$$

In Eq. 5, $2\pi bdb$ is the Coulomb scattering cross section (*17*), $P(b)$ is the probability of making a $1s\sigma$ vacancy during the collision, and dt has been replaced by dR/v_R, where v_R is the radial component of the projectile velocity, v_1. If the impact parameter of the collision is not defined, Eq. 5 has to be integrated over the appropriate range of impact parameters (*20*). A complete quantum mechanical calculation of the one-collision process is under way (*25*). It indicates that Eq. 5 is incomplete; there may also be an important contribution to the cross section due to transient effects.

Two-collision process. For a two-collision process, one has to consider that a projectile with a K vacancy has a probability $nv_1\tau_K 2\pi bdb$ of making a second collision (with impact parameter b) within the lifetime τ_K of the vacancy, where n is the atomic target density. Multiplying this probability by the jumping probability f of the K vacancy to the $1s\sigma$ MO (in the second collision) and by the radiative decay probability $dt/\tau_x(R)$, one obtains the probability of radiative MO decay of the incident projectile K vacancy. Hence, the differential yield of K MO x-ray emission with energy E_x is, per projectile K vacancy

$$d^2y^{(2)}/dE_x = 2nv_1\tau_K\, 2\pi bdbf(dR/dE_x)/v_R\tau_x(R) \quad (6)$$

A factor of 2 has been included because there are two crossings of a given R by a trajectory. [It would be more correct to consider the relevant interference effects, but these drop out on integration over impact parameters (*26*).] If the impact parameter b of the second collision is not defined, one must integrate Eq. 6 over the appropriate range of impact parameters, giving for the spectral yield per projectile K vacancy (*20, 27*)

$$dy^{(2)}/dE_x = 4\pi fn\tau_K(1 - D/R)^{1/2}R^2(dR/dE_x)/\tau_x(R) \quad (7)$$

where D is given by Eq. 3.

Quantum mechanical calculations for the two-collision process have been made (*22, 23, 28*). Although a detailed review of these calculations is not appropriate here, a sketch of the theory will be helpful for the subsequent discussion. The differential cross section for emission of a K MO x-ray with energy E_x ($= \hbar\omega$) in a collision with impact parameter b can be written (*22, 23*)

$$d^2\sigma/dE_x = 2\pi bdb \mid C(\omega,b) \mid {}^2\omega^2/(2\pi)^2\hbar c^3 \quad (8)$$

where C is the radiation amplitude, $\hbar$ is Planck's constant divided by 2π, c is the velocity of light, and, for simplicity, isotropy of the radiation with respect to the beam direction has been assumed. In the long-wavelength approximation one finds

$$C(\omega,b) = (-i/\hbar)\int_{-\infty}^{\infty} dt\, a(t)\, D_{fi}(t) \exp\{i\int^{t}[\omega - \omega_{fi}(t')]dt'\} \quad (9)$$

Here $a(t)$ is the amplitude for creating $1s\sigma$ vacancies, $D_{fi}(t)$ is the electric dipole (velocity) matrix element between the

initial (for example, $2p\pi$) and the final ($1s\sigma$) states, whose energy difference is denoted by $\hbar\omega_{fi}(t)$. For an exact treatment of the one-collision process the time coherence between $a(t)$ and the remaining radiation amplitude must be considered (*25*). For the two-collision process $|a(t)|^2$ is a constant representing the fractional number of $1s\sigma$ vacancies brought into the collision by the projectile. Müller and co-workers (*22, 23*) have obtained an analytical form for Eq. 9, making reasonable, simplifying assumptions for $D_{fi}(t)$ and $\omega_{fi}(t)$. At a fixed impact parameter b the quantity $|C(\omega,b)|^2$ is found to oscillate as a function of ω because of interference between the incoming and outgoing parts of the radiation amplitude [(*26*); see also (*29*) and (*30*)]. Upon integration over impact parameters, the oscillations effectively disappear (*22, 23, 28*), and for $E_x < E_{UA}$ the quasistatic approximation (*18*) turns out to be reasonably good. But for $E_x > E_{UA}$ important line-broadening effects are found (*21*), which can be represented by a spectral tail of the form

$$dy^{(2)}/dE_x \propto \exp(-E_x/\Gamma) \qquad (10)$$

where

$$\Gamma \approx 0.3\,[(E_{UA} - E_{SA})\hbar v_1/R_0]^{1/2} \qquad (11)$$

In Eq. 11 E_{UA} and E_{SA} are the UA and SA $K\alpha$ x-ray energies, respectively, and R_0 is approximately equal to twice the UA K radius.

Looking at Fig. 2, one can see that many different electronic transitions can fill a vacancy in the $1s\sigma$ MO. The $2p\pi \rightarrow 1s\sigma$ transition has the largest transition probability (*31*) and in most calculations is the only one taken into account. (At the SA and UA limits, the transition corresponds to a $K\alpha_1$ transition.)

Experimental Approaches

It is of interest to review the experimental evidence for the existence of MO x-rays as much as possible independent of any detailed theory, although finally only a detailed comparison can provide the assurance that the phenomenon is well understood. Since MO x-rays form continua one must consider other continua with which these might be confused and which might form backgrounds under the MO x-ray spectra (*19*). As shown below, by a suitable choice of collision partners and bombarding energy one can obtain spectra that consist almost entirely of background (for example, nucleus-nucleus bremsstrahlung radiation). Good agreement with the relevant theoretical cross sections (*32, 33*) permits calculation of the background in other situations. One can then choose conditions such that the x-ray continuum spectrum is due predominantly either to the two-collision process or to the one-collision process (*9, 10, 20, 34*). When the two-collision process is dominant, one can show that the K MO x-ray yield per projectile K vacancy has the expected dependence on the target density n. For the one-collision process it should be independent of n, but for the two-collision process it should be proportional to n (see Eq. 7) (*20*).

By using the Doppler effect it has been demonstrated, independent of any theory, that the continua assigned to MO x-rays are indeed emitted from the quasimolecular system consisting of projectile and target, and not from the target or projectile alone (*35, 36*). Calculations by Müller and co-workers (*37*) have stimulated measurements of the x-ray energy dependence of the anisotropy of MO x-ray continua with respect to the incident beam (*35, 36, 38, 39*). The peaking of the anisotropy near the UA limit also signals the quasimolecular origin of the continuum radiation (*38, 39*). The detailed interpretation of the anisotropy promises to yield important information about the x-ray emission process in heavy-ion collisions (*1, 2, 40*) and may contribute to an understanding of the spectroscopy of superheavy molecules (*6*).

Backgrounds

Various radiative processes due to electrons, bremsstrahlung of nuclei, and Compton scattering of gamma rays from nuclear excited states can form backgrounds under MO x-ray spectra, in addition to normal room background (*19, 41*). Figure 3 shows examples of different backgrounds.

Although non-MO, electronic radiative processes disturb MO spectra, they are of intrinsic interest and have been the subject of much theoretical and experimental study (*32, 42*). They are due main-

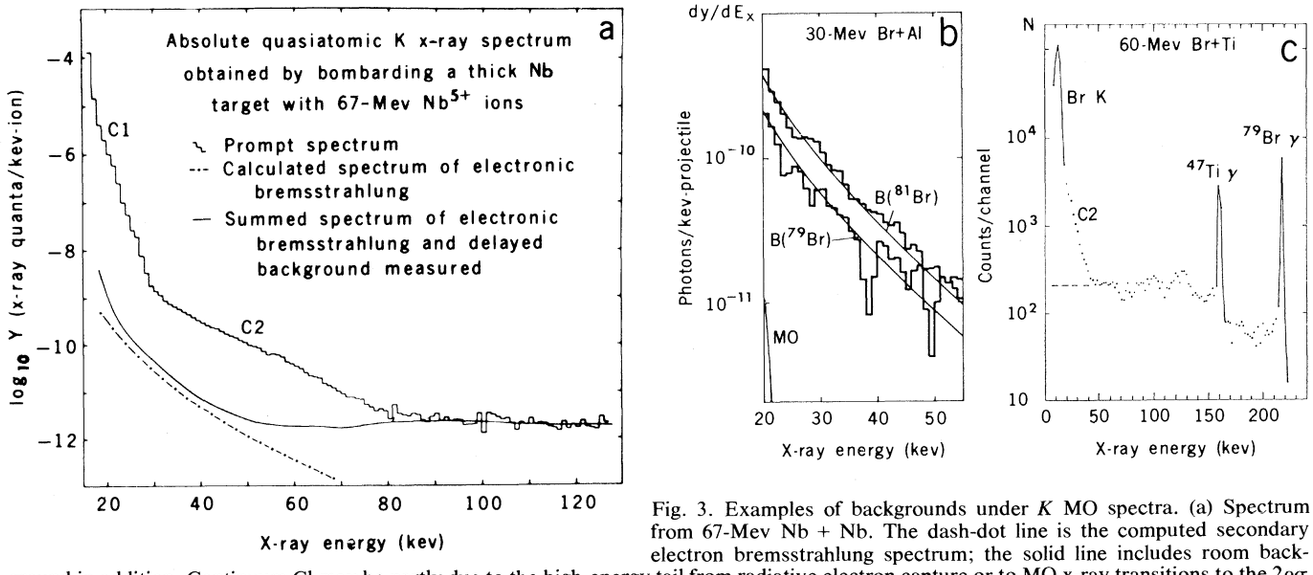

Fig. 3. Examples of backgrounds under K MO spectra. (a) Spectrum from 67-Mev Nb + Nb. The dash-dot line is the computed secondary electron bremsstrahlung spectrum; the solid line includes room background in addition. Continuum Cl may be partly due to the high-energy tail from radiative electron capture or to MO x-ray transitions to the $2p\sigma$ state. Continuum C2 is due to K MO x-rays (see Fig. 6c). [From Kaun (*44*)] (b) Spectra from 30-Mev ^{79}Br + Al and ^{81}Br + Al. The solid lines B are absolute computed nucleus-nucleus bremsstrahlung spectra for the two projectiles. In this experiment the MO contribution is very small. [From Meyerhof *et al.* (*47*)] (c) Spectrum from 60-Mev ^{79}Br + Ti. Nuclear gamma rays from ^{47}Ti and ^{79}Br can be seen. The dashed line is the extrapolation of the Compton continuum. Continuum C2 is due to K MO x-rays (see Fig. 6b). [From Meyerhof *et al.* (*47*)]

ly to loosely bound target electrons for which $v_1/v_e \gtrsim 1$ (see Eq. 1). One distinguishes radiative processes in which the target electron is captured into a vacant projectile state (radiative electron capture) or scattered by the projectile (primary electron bremsstrahlung or radiative ionization) from those in which the liberated target electron scatters on other target atoms (secondary electron bremsstrahlung or knock-on bremsstrahlung). The latter processes are particularly important in thick solid targets (*32, 42*), but their intensities turn out to be more than an order of magnitude below those of *K* MO x-ray spectra (*31, 43, 44*). For example, Fig. 3a shows a measured x-ray spectrum for 67-Mev Nb + Nb collisions (*43, 44*). The characteristic Nb *K* x-rays lie below 20 kev. The spectrum has been corrected for absorber and detection efficiency effects. The dash-dot line in Fig. 3a is the computed secondary electron bremsstrahlung spectrum, and the solid line includes the room background. One can see that the secondary electron bremsstrahlung is very small compared to the experimental continuum. (Nucleus-nucleus bremsstrahlung is negligibly small in this case.)

Primary electron bremsstrahlung forms a peaked spectrum centered around $E_x = \frac{1}{2}mv_1^2$ and radiative electron capture into the projectile *K* shell forms a peaked spectrum centered about $E_x = U_K + \frac{1}{2}mv_1^2$, where U_K is the projectile *K* ionization energy. For a typical projectile velocity of 10^9 centimeters per second, the energy $\frac{1}{2}mv_1^2$ is only 0.3 kev. Hence, as far as the study of *K* MO spectra is concerned, the important question is how intense the high-energy tails of these peaked spectra are. Unfortunately, calculations on this point are not yet definitive (*32, 42*). It is possible, though, that a sharply falling continuum, seen in many spectra just beyond the SA *K* lines, is at least partly due to radiative electron capture (for example, see Fig. 3a, continuum C1), but it has also been assigned to MO x-ray transitions ending on the $2p\sigma$ MO (*43–45*). In quite asymmetric collisions continuum spectra have recently been seen above the SA *K* lines, which do not agree with computed radiative electron capture or MO spectra (*46*). These may represent tails from primary electron bremsstrahlung.

Nucleus-nucleus bremsstrahlung may form a significant background under MO spectra (*19*), but the effect can be computed with good accuracy (*32, 33*). The electric dipole part of the cross section is proportional to $[(Z_1/A_1) - (Z_2/A_2)]^2$ where A_1 and A_2 are the mass numbers of the projectile and target, respectively. Hence, the intensity of the bremsstrahlung spectrum may vary markedly with the projectile isotope. Figure 3b shows thick target x-ray spectra from ^{79}Br + Al and ^{81}Br + Al and the corresponding (absolutely) computed nucleus-nucleus bremsstrahlung cross sections (*47*). The spectral yields differ by nearly a factor of 2. The good fit between theory and experiment allows theoretical nucleus-nucleus bremsstrahlung spectra to be computed in less obvious situations (see below). For identical projectile and target isotopes, the electric dipole cross section is zero, but in cases where the dipole cross section is small, dipole-quadrupole interference can be of major importance (*32, 33*).

Figure 3c gives an illustration of background due to Coulomb-excited nuclear gamma rays from 60-Mev ^{79}Br + Ti (*47*). In this case, the x-rays were detected in a 17-cm^3 coaxial Ge(Li) detector, with no additional absorber. To determine the shape of the background under the x-ray continuum one can use gamma rays of similar energy from a radioactive source. The background is quite flat, so the accuracy of the extracted x-ray continuum is affected only at the high-energy part of the spectrum. One can minimize this type of background by using projectiles and targets with nuclei having high-lying excited states.

K Molecular Orbital X-ray Spectra

One can produce *K* MO x-ray spectra under conditions where the two-collision and the one-collision processes are separately dominant. One can show that because of the factor f in Eq. 7 the two-collision process is strongest for symmetric collisions (*20*). Also, it turns out that the dependence of the two- or one-collision process on the projectile energy is determined mainly by the cross section for making vacancies in the $2p\sigma$ or $1s\sigma$ state, respectively (*20*). Since the cross section rises more steeply with energy in the latter case (*48*), the two-collision process will dominate only at a sufficiently low bombarding energy, which depends on the particular collision system.

Figure 4a shows the continuum spectrum from 30-Mev Br + Br (*20*). The SA Br *K* x-rays lie near 12 kev and the continuum C1 (compare Fig. 3a) disappears near 20 kev. Above that energy, the continuum spectrum agrees in absolute magnitude with the two-collision quasistatic calculation (curve *T* in Fig. 4a) (Eq. 6), as well as with the full quantum mechanical treatment (curve *TQ*) (*22, 23*). The one-collision process (curve *O*) and the nucleus-nucleus bremsstrahlung contribution due to the mixture of isotopes in the target (curve

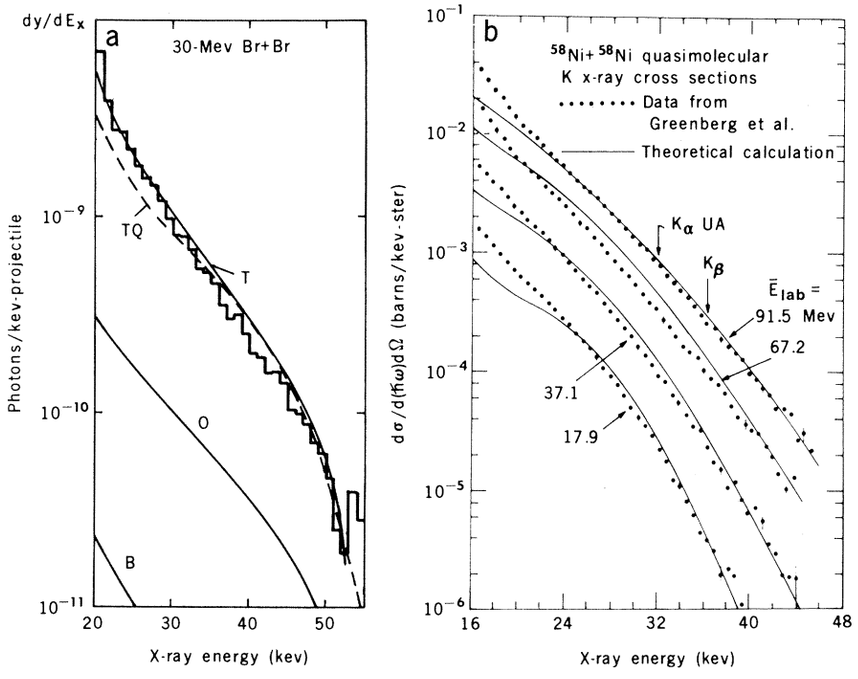

Fig. 4. Spectra of *K* MO x-rays from collisions in which the two-collision process is dominant. (a) Spectra for 30-Mev Br + Br. The histogram shows experimental data. The curves are absolute calculations based on two-collision quasistatic theory (*T*) (Eq. 6), two-collision quantum mechanical theory (*TQ*) [from Müller (*23*)], the one-collision quasistatic process (*O*), and nucleus-nucleus bremsstrahlung (*B*). [From Meyerhof *et al.* (*20*)] (b) Spectra for ^{58}Ni + ^{58}Ni at various bombarding energies [from Greenberg (*49*)]. The curves are absolute two-collision quantum mechanical calculations. Note the dynamic tail beyond the UA limit [from Müller (*23*)].

B) are very small in this case. Figure 4b gives several spectra for $^{58}Ni + ^{58}Ni$ (*49*). The quantum mechanical two-collision calculations agree with the experimental spectra well beyond the UA limit (*22, 23*). These spectra demonstrate the importance of the dynamic tail (Eq. 10). The absolute fits in Fig. 4 provide one important piece of evidence for the existence of *K* MO spectra, as well as for the role of the two-collision process.

Two other independent confirmations of the two-collision process are available: using gas targets and comparing spectra from $N^+ + N_2$ and $N^+ + NH_3$ (in the bombarding energy range from 35 to 400 kev), Saris and co-workers (*9, 10*) have found the $N^+ + N_2$ spectra to be by far the most intense. The explanation is that the N^+ projectile can obtain a *K* vacancy in a collision with one N target atom and then carry the vacancy into a collision with the second target atom in the N_2 molecule. In NH_3 the H atoms are not very effective in producing *K* vacancies.

In experiments with solid targets containing Br, in which the Br concentration was varied, a series of spectra were obtained with 30-Mev Br projectiles, as shown in Fig. 5a. The relative atomic Br concentration, n_{rel}, is indicated, with unity representing a solid (frozen) Br target. The other constituents in the target (K and Cl) contribute to the MO spectra only in a minor way. Each spectrum is fitted absolutely with the sum of two-collision (*T*), one-collision (*O*), and nucleus-nucleus bremsstrahlung (*B*) contributions. After the latter two have been subtracted from the spectra, the remainders are integrated over energy and plotted against the relative Br concentration (Fig. 5b). The expected proportionality to *n* (Eq. 7) is found, confirming the importance of the two-collision mechanism in this case.

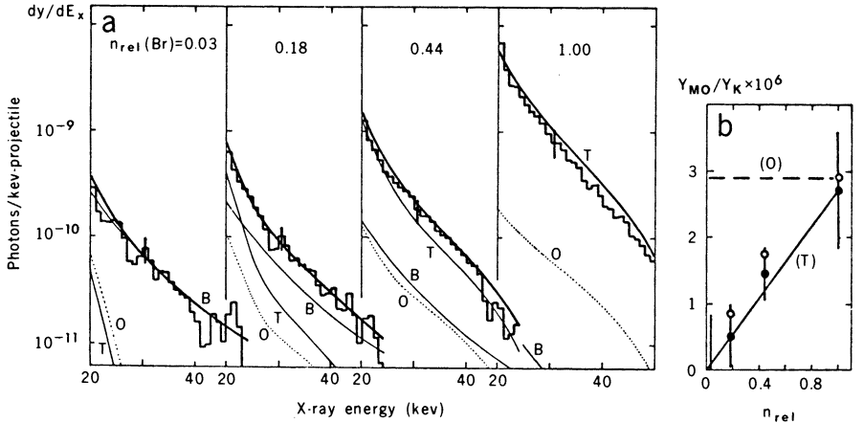

Fig. 5. (a) Corrected x-ray spectra from bombardment of various Br targets with 30-Mev Br. Room background has been subtracted. Typical systematic errors are ± 30 percent. The relative Br densities, n_{rel}(Br), correspond to the following targets: 1.00, pure Br; 0.44, pure KBr; 0.18, 50 percent KBr + 50 percent KCl; 0.03, 10 percent KBr + 90 percent KCl. In each case, *B*, *O*, and *T* are the computed bremsstrahlung and one- and two-collision MO spectra, respectively. The darker curves give *B* + *O* + *T*. (b) Ratio of integrated MO *K* x-ray yield (E_x = 27 to 50 kev) to beam *K*-vacancy yield plotted against relative Br density. Lines *O* and *T* give the relationships expected for one- and two-collision mechanisms, respectively. Open symbols represent total MO yield, solid symbols total MO yield minus estimated one-collision contribution. [From Meyerhof *et al.* (*20*)]

Figure 6 shows various spectra in which the one-collision process is expected to dominate. The most direct evidence for the one-collision process comes from the use of monatomic gas targets (*34*), with which the two-collision mechanism cannot contribute. The distance between target atoms in a gas is too large for the projectile *K* vacancy to survive between collisions (see the discussion preceding Eq. 6). Figure 6a shows the x-ray spectrum from 48-Mev S + Ne (*34*). Here strong dynamic effects are expected beyond the UA limit, but still the spectrum agrees within an order of magnitude with the quasistatic one-collision prescription of (*20*). Figure 6b shows the continuum spectrum from Fig. 3c after subtraction of background and correction for absorber and detection efficiency effects. Figure 6c gives the spectrum from Fig. 3a after background is subtracted. In Fig. 6, b and c, the one-collision process (curve *O*) appears to dominate over the (quasistatic) two-collision and nucleus-nucleus bremsstrahlung spectra (curves *T* and *B*, respectively). Figure 6 leaves no doubt that the two-collision process alone cannot explain the spectra. A quantum mechanical treatment of the one-collision process is needed (*25*); meanwhile, one has to contend with a quasistatic prescription for the one-collision spectrum (*20*).

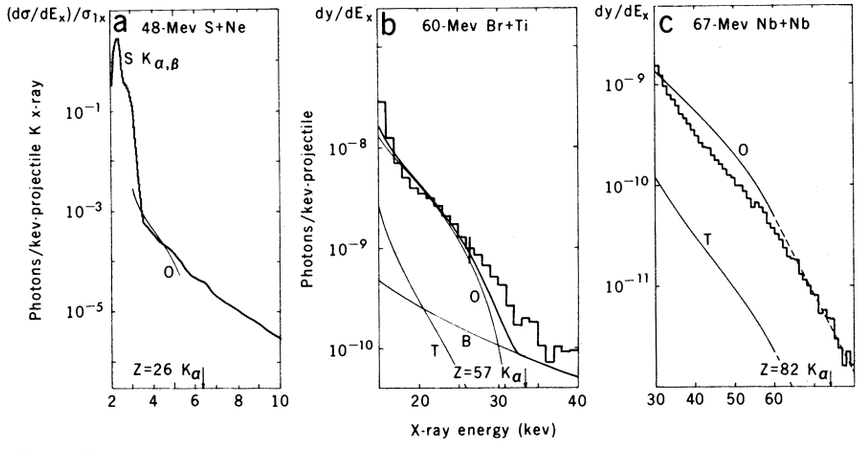

Fig. 6. Continuum x-ray spectra from collisions in which the one-collision MO x-ray process is expected to be dominant. (a) Spectrum for 48-Mev S + Ne (gas target). The quasistatic one-collision prediction (*O*) is shown. [From Bell *et al.* (*34*)] (b) Spectrum for 60-Mev Br + Ti (see Fig. 3c). Curves *O* and *T* represent the quasistatic one- and two-collision predictions, curve *B* the nucleus-nucleus bremsstrahlung spectrum, and the heavy line their sum. [From Meyerhof *et al.* (*20*)] (c) Spectrum for 67-Mev Nb + Nb. The notation is the same for (b), except that expected dynamic tail (Eq. 10) is indicated by a dashed line. [From Kaun (*44*)]

L and *M* Molecular Orbital X-ray Spectra

Although *L* MO x-rays were the first MO x-rays to be discovered (*7, 8*), it has not yet been possible to make the same kind of quantitative fit to *L* MO x-ray spectra as to the *K* spectra (Figs. 4 to 6). This is because the *L* spectra consist of several, roughly equally intense, MO transitions (*31*). In addition, the transition energies are strongly influenced by the state of ionization of the projectile-target system (*50*). So far, one has succeeded in establishing regularities in the variation of the approximate "end point" of *L* MO spectra (*51*). Also, it appears that there

can be one- and two-collision processes of L MO x-ray production (see Fig. 1b) (*9, 10*). Figure 7a shows the spectrum from 88-Mev Pb + Pb collisions (*47*), as seen in a 4-millimeter intrinsic Ge detector. This particular detector was too small to detect the SA K lines from Pb. But there is a rapidly falling continuum beyond the SA L spectrum, which disappears into room background above ~ 60 kev. This energy is just the ionization energy for the $2p_{3/2}\pi$ state of the quasimolecule $Z_1 + Z_2 = 164$ at R_{min} (Eq. 2) (*47, 50*), which suggests that this continuum may be the L MO x-ray spectrum for $Z_{UA} = 164$. Substituting the appropriate energies into Eq. 11 gives the dynamic tail shown as a dashed line in Fig. 7a; the slope is close to that of the experimental spectrum.

One interesting feature of M MO spectra is that, despite a multitude of possible x-ray emitting transitions, they are peaked (see Fig. 1a), in contrast to K and L MO spectra, which fall roughly exponentially with energy (*3–5*). This is because over a considerable span of the internuclear distance R, the transition energy is practically independent of R (for example, see the $4f\sigma \rightarrow 3d\pi$ transition for $R < 0.1$ atomic unit in Fig. 2c). Since the MO spectral distribution, in the quasistatic approximation, depends on dR/dE_x (Eqs. 4 to 6), one expects a sharp peaking which is somewhat abated, but not completely eliminated, by line-broadening effects (*3–5*). There are still difficulties in explaining the absolute intensity of M MO spectra (*3–5*), but the peaking feature permits spectroscopic studies of superheavy quasimolecules. Figure 7b shows x-ray spectra for 11-Mev I colliding with a variety of targets (*3–5*). Above an x-ray energy of 5 kev the absorber hardly affects the spectra. The arrows in Fig. 7b indicate computed UA $4f \rightarrow 3d$ transition energies (*5, 15, 50*); the good agreement with experiment shows that it may be possible to extract spectroscopic information from M MO spectra.

The Radiating System

The Doppler shift of the continuum spectrum can be used to determine the nature of the radiating system in a way that is independent of any detailed model of the collision process (*35, 36*). It follows from symmetry principles that in the center-of-mass (CM) system of the emitter the radiation cannot show any fore-aft asymmetry (*37*). In the laboratory system, the Doppler shift affects the energy, angle, and solid angle of the radiation. Even if the angular distribution of the radiation in the CM system is not known, one can use the fact that it must be symmetric about 90° in order to extract the Doppler velocity as a function of E_x.

Figure 8a shows an x-ray spectrum from 200-Mev Kr + Zr (*35*). The SA x-rays lie below 18 kev. Nucleus-nucleus bremsstrahlung is negligibly small in this case. The shape and intensity of the spectrum are mainly due to the one-collision process (solid line). The dotted line gives the dynamic tail (Eq. 10) fitted to the spectrum above the UA limit. The ex-

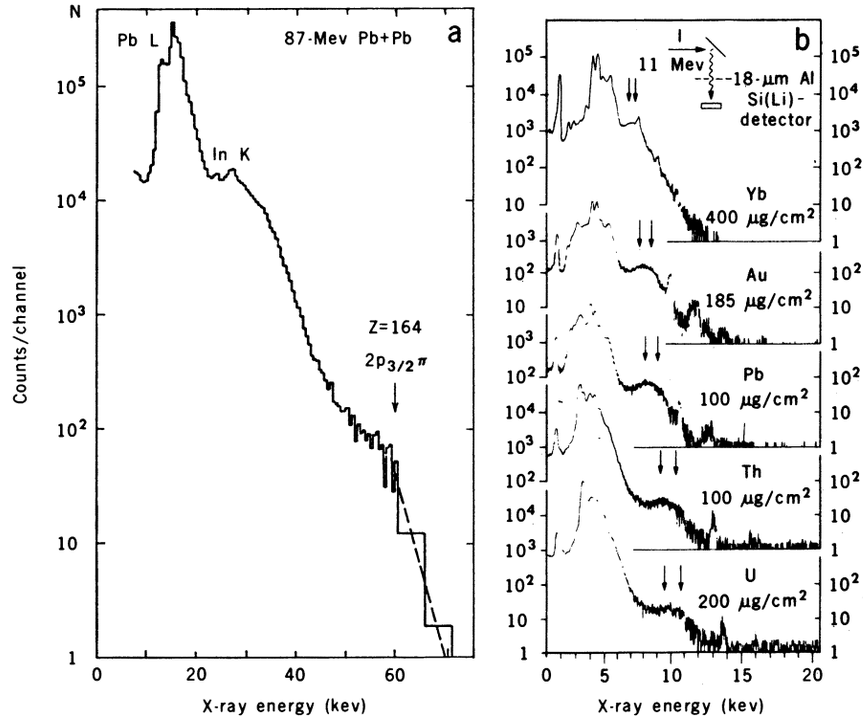

Fig. 7. (a) X-ray spectrum from 88-Mev Pb + Pb. An intrinsic Ge detector with a 1.6-mm Al absorber was used. Below 40 kev the spectrum is severely distorted by the absorber. Only room background has been subtracted. Small fluorescent K x-ray peaks due to In metal used in the detector can be seen. The $2p_{3/2}\pi$ binding energy for $Z = 164$ is shown. The dashed line gives the slope of the dynamic tail, assuming that the continuum is due to $L\alpha$ Mo x-rays. [From Meyerhof *et al.* (*47*)] (b) X-ray spectra from bombardment of a variety of thin targets with 11-Mev I. The arrows indicate computed UA $4f \rightarrow 3d$ transition energies about which the M MO x-ray spectra appear to be centered. The peak structure around 5 kev is the absorber-distorted L x-ray spectrum of I, and the small peaks near 10 to 14 kev are from target L x-rays. [From Mokler *et al.* (*4*)]

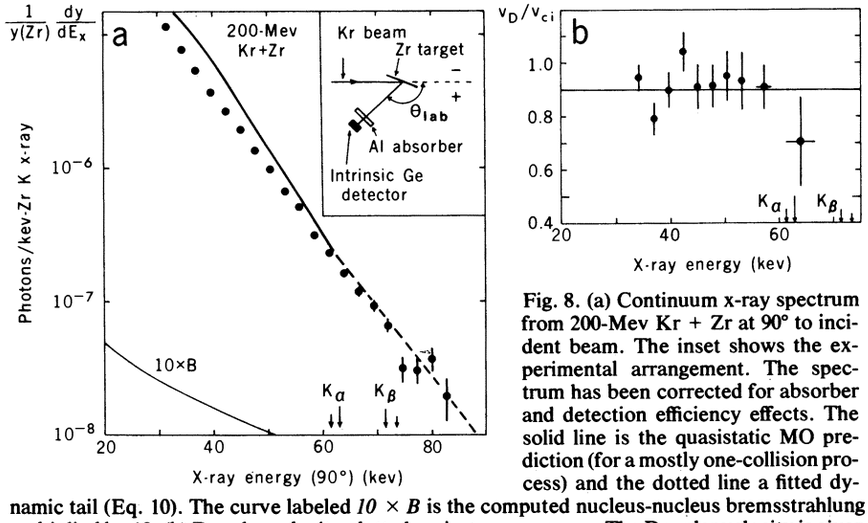

Fig. 8. (a) Continuum x-ray spectrum from 200-Mev Kr + Zr at 90° to incident beam. The inset shows the experimental arrangement. The spectrum has been corrected for absorber and detection efficiency effects. The solid line is the quasistatic MO prediction (for a mostly one-collision process) and the dotted line a fitted dynamic tail (Eq. 10). The curve labeled $10 \times B$ is the computed nucleus-nucleus bremsstrahlung multiplied by 10. (b) Doppler velocity plotted against x-ray energy. The Doppler velocity is given in units of the CM velocity of the incident Kr + Zr quasimolecule. The horizontal line is the expected velocity ratio, assuming that the continuum is emitted by the Kr + Zr quasimolecule. [From Meyerhof *et al.* (*35*)]

tracted Doppler velocity v_D is shown in Fig. 8b as a function of the x-ray energy. It is given in terms of the velocity v_{ci} of the Kr + Zr quasimolecule, assuming the projectile has the incident velocity. Because of the slowing down of the Kr projectile in the thick Zr target, the average ratio v_D/v_{ci} is expected to be 0.90, assuming the quasimolecule is the emitter of the continuum radiation. This agrees well with the experimental average value 0.92 ± 0.03 obtained from Fig. 8b. If the target were the emitter one should find $v_D/v_{ci} \approx 0$, and if the projectile were the emitter one should find $v_D/v_{ci} \approx 1.9$. Similar results have been found for M MO radiation (*36*).

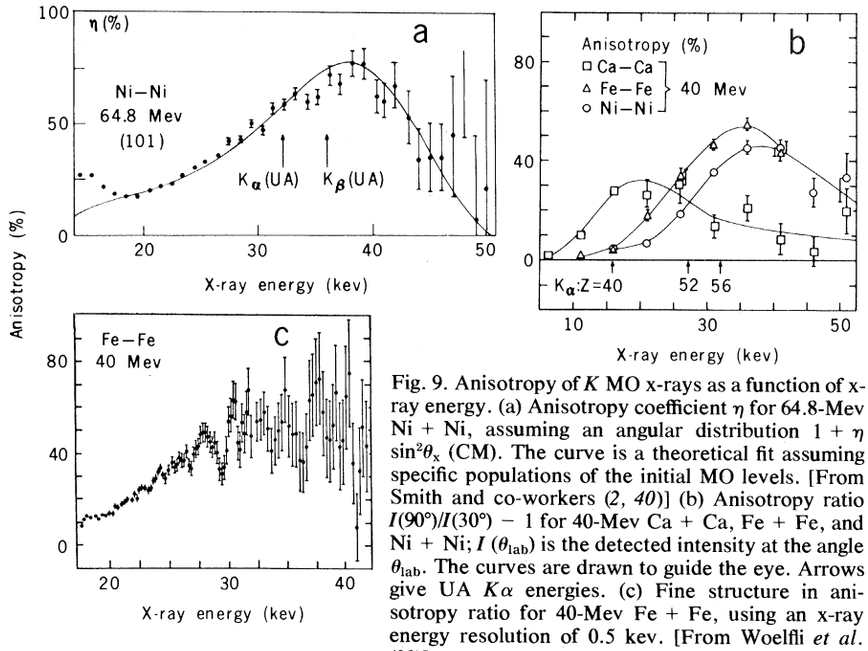

Fig. 9. Anisotropy of K MO x-rays as a function of x-ray energy. (a) Anisotropy coefficient η for 64.8-Mev Ni + Ni, assuming an angular distribution $1 + \eta \sin^2\theta_x$ (CM). The curve is a theoretical fit assuming specific populations of the initial MO levels. [From Smith and co-workers (*2, 40*)] (b) Anisotropy ratio $I(90°)/I(30°) - 1$ for 40-Mev Ca + Ca, Fe + Fe, and Ni + Ni; $I(\theta_{lab})$ is the detected intensity at the angle θ_{lab}. The curves are drawn to guide the eye. Arrows give UA $K\alpha$ energies. (c) Fine structure in anisotropy ratio for 40-Mev Fe + Fe, using an x-ray energy resolution of 0.5 kev. [From Woelfli *et al.* (*39*)]

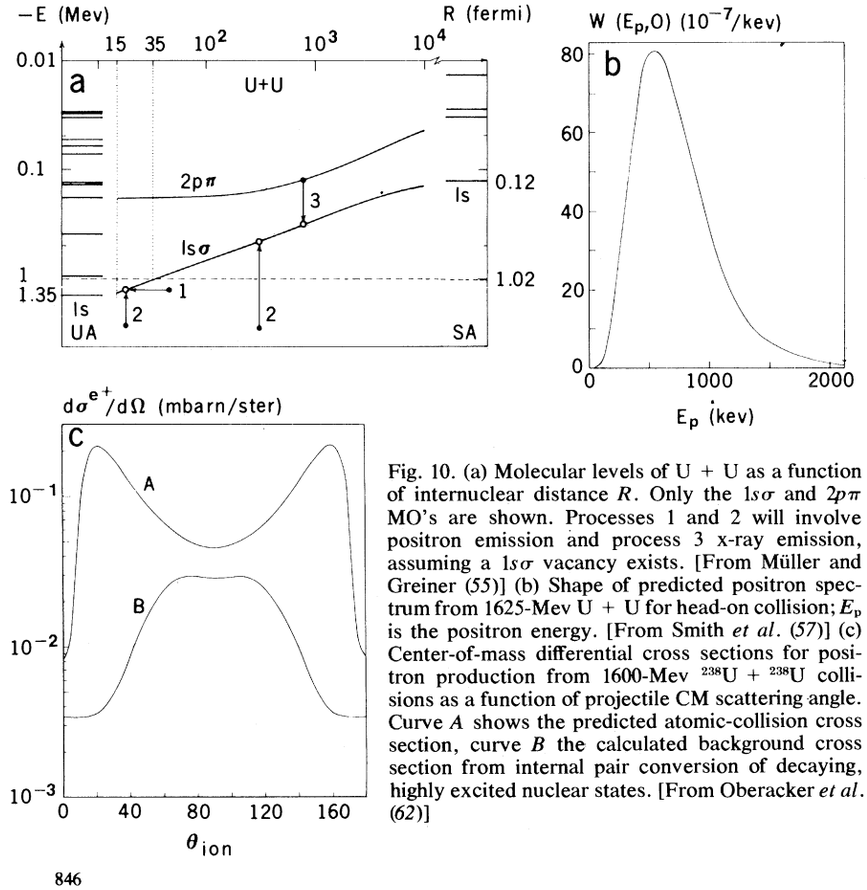

Fig. 10. (a) Molecular levels of U + U as a function of internuclear distance R. Only the $1s\sigma$ and $2p\pi$ MO's are shown. Processes 1 and 2 will involve positron emission and process 3 x-ray emission, assuming a $1s\sigma$ vacancy exists. [From Müller and Greiner (*55*)] (b) Shape of predicted positron spectrum from 1625-Mev U + U for head-on collision; E_p is the positron energy. [From Smith *et al.* (*57*)] (c) Center-of-mass differential cross sections for positron production from 1600-Mev $^{238}U + ^{238}U$ collisions as a function of projectile CM scattering angle. Curve A shows the predicted atomic-collision cross section, curve B the calculated background cross section from internal pair conversion of decaying, highly excited nuclear states. [From Oberacker *et al.* (*62*)]

Anisotropy of Molecular Orbital Radiation

Experimental searches for an anisotropy of MO radiation with respect to the beam direction were stimulated by Müller and co-workers (*37*). The calculations, based on a quasistatic model, indicated that the Coriolis coupling of the emitting electron in the rotating quasimolecule should give a significant anisotropic contribution to MO radiation. The additional radiation is called induced, to distinguish it from the spontaneously emitted radiation from a fixed quasimolecule, which may also be an anisotropic. The overall angular distribution of the radiation is found to be $1 + \eta \sin^2\theta_x$ where θ_x is the angle of the emitted x-ray with respect to the incident beam in the CM system and η depends on E_x. Experiments indeed reveal an anisotropy for K, L, and M MO radiation that is dependent on x-ray energy (*35, 36, 38, 39*). The anisotropy peaks near the UA limit, signaling the quasimolecular origin of the radiation. The original calculations (*37*) also showed that the anisotropy of the induced radiation should peak sharply near the UA limit. New, quantum mechanical, calculations indicate that the induced radiation is not as important as was originally believed. The anisotropies may be predominantly due to unequal population of the initial MO levels, which can produce a large anisotropy of the spontaneous radiation, also peaking near the UA limit (*1, 2, 40*).

Figure 9 shows various interesting features of the anisotropy. Figure 9a shows the anisotropy of the K MO spectrum from 64.8-Mev Ni + Ni (see Fig. 4b) found by Greenberg *et al.* (*38*) and a theoretical fit by Smith and co-workers (*2, 40*), which assumes that the initial $2p_{3/2}\sigma$ state is completely empty and the $2p_{3/2}\pi$ and $2p_{1/2}\sigma$ states completely full. A theoretical reason for these assumptions is not yet available. Figure 9, b and c, are from the work of Woelfli and co-workers (*39*). Figure 9b shows that in diverse collision systems the anisotropy indeed peaks near the UA $K\alpha$ limit (arrows on the abscissa); the curves are drawn to guide the eye. The peaking of the anisotropy near the UA $K\alpha$ limit may permit spectroscopic studies of the $1s\sigma$ MO even in superheavy quasimolecules (*6*). Figure 9c shows an oscillating fine structure in the anisotropy; at present this is unexplained, but it may be connected

with coherence effects in the radiative amplitude for MO x-ray emission, similar to those suggested in (*52*), or with a possible splitting of MO levels caused by the rotation of the quasimolecule (*39*).

Impact Parameter Dependence

By detecting projectiles scattered at a particular angle in coincidence with MO x-rays, the impact parameter of the collision can be specified (*17*). In the quasistatic theory the spectral shape should be given by Eqs. 5 or 6. Because of the occurrence of the reciprocal of the radial component v_R of the projectile velocity, the quasistatic theory predicts a sharp peak at the (highest) x-ray energy corresponding to $R = R_{\min}$ (Eq. 2), where $v_R = 0$. Quantum mechanical calculations for the two-collision spectrum predict a line-broadened peak, as well as oscillatory structure in the spectrum due to interference effects in the radiation amplitude between the incident and outgoing parts of the collision (Eqs. 8 and 9) (*22, 23, 28–30, 40*).

Coincidence experiments between MO x-rays and scattered projectiles are very tedious because of the small intensity of the MO radiation. No oscillating structure has been seen in the few measurements made to date, nor has the predicted peaking near the UA limit been found in K and M MO spectra (*53*). Answers to these puzzling problems remain to be found.

Positron Emission: An Open Question

One exciting open question is whether the predicted positrons from the decay of deep inner-shell vacancies of superheavy quasimolecules can be detected (*1, 2*). It has been suggested that such positrons should be emitted in energetic U + U collisions (*1, 2*). Figure 10a gives a simplified MO correlation diagram for the U + U system (*54, 55*). For $R \gtrsim 35$ fermis the $1s\sigma$ MO dives into the negative energy continuum of the Dirac theory. Should a vacancy exist in the $1s\sigma$ MO, electrons from the negative energy continuum, rather than from higher MO levels (process 3 in Fig. 10a), can fill the vacancy, thereby liberating positrons (*56*) (process 1 in Fig. 10a). This process is of fundamental significance because it can be considered as the breakdown of the vacuum state under the influence of extremely high electric fields (*1, 2*).

Dynamic effects in the collision enhance the yield strongly, since there can be an energy transfer from the nuclear motion to the electrons, allowing transitions from the negative energy continuum into $1s\sigma$ vacancies even before diving occurs (process 2 in Fig. 10a) (*57*). Figure 10b shows the predicted shape of the positron spectrum at fixed impact parameter b ($b = 0$) for 1625-Mev U + U collisions. In terms of the shape function $W(E_p,b)$ the differential cross section for emission of positrons of energy E_p is

$$d^2\sigma_p/dE_p = L_0 2\pi b db\, W(E_p,b)$$

where L_0 is the fraction of projectiles with a $1s\sigma$ vacancy. This expression assumes no coherence between the amplitude for creating $1s\sigma$ vacancies and the decay amplitude, an assumption which is not accurate if the process goes by the one-collision mechanism (*22, 23*).

From an experimental point of view, the possibility of detecting positrons depends on the magnitude of L_0 and on possible background positrons. In the quasistatic approximation, the value of L_0 is given by $P(b << a_K)$ if a one-collision process occurs, or by $nv_1\tau_K\sigma_K$ if a two-collision process occurs (see Eqs. 5 and 6), where σ_K is the cross section for projectile K vacancy production. For 1600-Mev U + U, the value of $P(0)$ has been estimated from cross-section systematics, based on the atomic model, to be 0.2 (*58*), whereas nonrelativistic systematics based on the molecular model lead to values between 10^{-4} and 10^{-5}, depending on the method of extrapolation (*48, 59*). Relativistic effects may enhance the latter estimates by several orders of magnitude (*60*). On the other hand, for this collision, $nv_1\tau_K\sigma_K \approx 4 \times 10^{-10}$ (*61*), so the two-collision process is expected to be negligible.

Calculations show that the largest positron background is due to internal pair conversion from the decay of highly excited nuclear states in U (*62*). Figure 10c shows the predicted positron differential cross section for 1600-Mev $^{238}U + ^{238}U$ collisions as a function of the projectile CM scattering angle (curve A). A value $L_0 = 10^{-2}$ is assumed. Curve B gives the estimated positron background due to internal pair conversion. For unequal U nuclei, the background is estimated to be smaller. Hence detection of positrons from heavy-ion collisions, although very difficult, appears to be feasible (*1, 2*).

Summary

The discovery and investigation of x-ray continua has provided a new tool for studying the detailed electronic processes that occur when atoms collide. In the collisions considered here, the quasimolecular origin of the continuum radiation has been established. Therefore, as the atomic numbers of the projectiles and target atoms are increased one can simulate some of the properties of superheavy atoms. In particular, the peaked nature of the x-ray energy dependence of the anisotropy of K, L, and M MO radiation, as well as the peaked nature of the M MO spectra, will allow approximate spectroscopic studies of superheavy atoms. Special excitement attaches to the possibility of observing fundamental processes occurring under extremely high electric and magnetic fields. The recent successful development of a 1400-Mev U beam at the GSI (Gesellschaft für Schwerionenforschung) accelerator in Darmstadt, Germany, promises an imminent attack on these basic problems (*63*).

References and Notes

1. J. Rafelski, L. Fulcher, W. Greiner, *Phys. Rev. Lett.* **27**. 958 (1971); J. Rafelski and B. Müller, *ibid.* **36**, 517 (1976).
2. W. Betz, G. Heiligenthal, J. Reinhardt, R. K. Smith, W. Greiner, in *The Physics of Electronic and Atomic Collisions*, J. S. Risley and R. Geballe, Eds. (Univ. of Washington Press, Seattle, 1975), p. 531.
3. P. H. Mokler, H. J. Stein, P. Armbruster, *Phys. Lett.* **29**, 827 (1972); B. Fricke and J. T. Waber, *Phys. Rev. C* **8**, 330 (1973); H. O. Lutz, W. R. McMurray, R. Pretorius, I. J. Van Heerden, R. J. Van Reenen, B. Fricke, *J. Phys. B* **9**, L157 (1976).
4. P. H. Mokler, *et al.* in *Atomic Physics*, G. zu Putlitz, E. W. Weber, A. Winnacker, Eds. (Plenum, New York, 1975), vol. 4, p. 301.
5. B. Fricke, R. Rashid, P. Bertoncini, A. C. Wahl, *Phys. Rev. Lett.* **34**, 243 (1975).
6. B. Müller, R. K. Smith, W. Greiner, *Phys. Lett. B* **53**, 401 (1975).
7. F. W. Saris, W. F. van der Weg, H. Tawara, R. Laubert, *Phys. Rev. Lett.* **28**, 717 (1972).
8. For more recent references see Mokler *et al.* (*4*) and W. E. Meyerhof, in *The Physics of Electronic and Atomic Collisions*, J. S. Risley and R. Geballe, Eds. (Univ. of Washington Press, Seattle, 1975), p. 470.
9. T. P. Hoogkamer, P. Worlee, C. Foster, F. Saris, in *Abstracts, 9th International Conference on the Physics of Electronic and Atomic Collisions*, J. S. Risley and R. Geballe, Eds. (Univ. of Washington Press, Seattle, 1975), p. 300.
10. W. E. Meyerhoff, Th. P. Hoogkamer, F. W. Saris, *Abstracts, Fifth International Conference on Atomic Physics*, R. Marrus, M. H. Prior, H. A. Shugard, Eds. (Univ. of Calif. Press, Berkeley, 1976), p. 56.
11. J. R. MacDonald, M. D. Brown, T. Chiao, *Phys. Rev. Lett.* **30**, 471 (1973).
12. This subject is reviewed by D. H. Madison and E. Merzbacher, in *Atomic Inner-Shell Processes*, B. Craseman, Ed. (Academic Press, New York, 1975), p. 1. A historical summary and many experimental methods and results are given by P. Richard, in *ibid.*, p. 73. See also J. M. Hansteen, in *Advances in Atomic and Molecular Physics*, D. R. Bates and B. Bederson, Eds. (Academic Press, New York, 1975), vol. 11, p. 299; J. D. Garcia, R. J. Fortner, T. M. Kavanagh, *Rev. Mod. Phys.* **45**, 111 (1973); Q. C. Kessel and B. Fastrup, *Case Stud. At. Phys.* **3**, 137 (1973); W. Brandt, in *Atomic Physics*, S. J. Smith and G. K. Walters, Eds. (Plenum, New York, 1972), vol. 3, p. 155; J. S. Briggs, *Rep. Prog. Phys.* **39**, 217 (1976).
13. U. Fano and W. Lichten, *Phys. Rev. Lett.* **14**, 627 (1965); M. Barat and W. Lichten, *Phys. Rev. A* **6**, 211 (1972); W. Lichten, in *Atomic Physics*, G. zu Putlitz, E. W. Weber, A. Winnacker, Eds. (Plenum, New York, 1975), vol. 4, p. 249.
14. G. Basbas, W. Brandt, R. Laubert, *Phys. Rev. A* **7**, 983 (1973); G. Basbas, W. Brandt, R. M. Ritchie, *ibid.*, p. 1971; W. Brandt and G. Lapicki, *ibid.* **10**, 474 (1974).
15. Calculations for the I + Au system have now

been extended to 56 electrons by A. Rosén, D. Ellis, B. Fricke, and T. Morović [in *Abstracts, Second International Conference on Inner-Shell Ionization Phenomena*, W. Mehlhorn, Ed. (University of Freiburg, Freiburg, Germany, 1976), p. 18].
16. M. Barat, in *The Physics of Electronic and Atomic Collisions*, B. C. Cobic and M. V. Kurepa, Eds. (Institute of Physics, Belgrade, Yugoslavia, 1973), p. 43; R. McCarroll, in *ibid.*, p. 71.
17. R. D. Evans, *The Atomic Nucleus* (McGraw-Hill, New York, 1955), p. 845.
18. W. Bambynek, B. Crasemann, R. W. Fink, H. V. Freund, H. Mark, R. E. Price, P. V. Rao, *Rev. Mod. Phys.* **44**, 716 (1972).
19. C. K. Davis and J. S. Greenberg, *Phys. Rev. Lett.* **32**, 1215 (1974); T. K. Saylor, personal communication.
20. W. E. Meyerhof, T. K. Saylor, S. M. Lazarus, A. Little, B. B. Triplett, L. F. Chase, Jr., R. Anholt, *Phys. Rev. Lett.* **32**, 1279 (1974).
21. H. D. Betz, F. Bell, H. Panke, W. Stehling, E. Spindler, M. Kleber, *ibid.* **34**, 1256 (1975).
22. K. Smith, B. Müller, W. Greiner, *J. Phys. B* **8**, 75 (1975).
23. B. Müller, in *The Physics of Electronic and Atomic Collisions*, J. S. Risley and R. Geballe, Eds. (Univ. of Washington Press, Seattle, 1975), p. 481.
24. W. E. Meyerhof, *Phys. Rev. Lett.* **31**, 1341 (1973); K. Taulbjerg, J. Vaaben, B. Fastrup, *Phys. Rev. A* **12**, 2325 (1975).
25. W. R. Thorson and S. H. Choi, in *Abstracts, 9th International Conference on the Physics of Electronic and Atomic Collisions*, J. S. Risley and R. Geballe, Eds. (Univ. of Washington Press, Seattle, 1975), p. 298; personal communication.
26. K. Smith and W. Greiner, *J. Phys. B*, in press.
27. J. S. Briggs, *ibid.* **7**, 47 (1974).
28. J. H. Macek and J. S. Briggs, *ibid.*, p. 1312.
29. W. Lichten, *Phys. Rev. A* **9**, 1458 (1974).
30. J. S. Briggs, *J. Phys. B*, in press.
31. R. Anholt, unpublished results.
32. D. H. Jakubassa and M. Kleber, *Z. Phys. A* **273**, 29 (1975).
33. K. Alder, A. Bohr, T. Huus, B. Mottelson, A. Winther, *Rev. Mod. Phys.* **28**, 432 (1956); J. Reinhardt, G. Soff, W. Greiner, *Z. Phys. A* **276**, 285 (1976); H. P. Trautvetter, J. S. Greenberg, P. Vincent, *Phys. Rev. Lett.* **37**, 202 (1976).
34. F. Bell, H. D. Betz, H. Panke, E. Spindler, W. Stehling, M. Kleber, *ibid.* **35**, 841 (1975).
35. W. E. Meyerhof, T. K. Saylor, R. Anholt, *Phys. Rev. A* **12**, 2641 (1975).
36. P. H. Mokler, P. Armbruster, F. Folkman, S. Hagmann, G. Kraft, H. J. Stein, in *The Physics of Electronic and Atomic Collisions*, J. S. Risley and R. Geballe, Eds. (Univ. of Washington Press, Seattle, 1975), p. 501; F. Folkmann, P. Armbruster, S. Hagmann, G. Kraft, P. H. Mokler, H. J. Stein, *Z. Phys. A* **276**, 15 (1976).
37. B. Müller, R. K. Smith, W. Greiner, *Phys. Lett. B* **49**, 219 (1974); B. Müller and W. Greiner, *Phys. Rev. Lett.* **33**, 469 (1974); M. Gros, B. Müller, W. Greiner, *J. Phys. B*, in press.
38. J. S. Greenberg, C. K. Davis, P. Vincent, *Phys. Rev. Lett.* **33**, 473 (1974).
39. W. Woelfli, C. Stoller, G. Bonani, M. Suter, M. Stoeckli, *Lett. Nuovo Cimento* **14**, 577 (1975); W. Woelfli, C. Stoller, G. Bonani, M. Stoeckli, M. Suter, *Phys. Rev. Lett.* **36**, 309 (1976).
40. R. K. Smith, paper presented at the Fourth International Seminar on Ion-Atom Collisions, Stanford University, 1975; _____ and W. Greiner, in preparation.
41. F. Folkmann, C. Gaarde, T. Huus, K. Kemp, *Nucl. Instrum. Methods* **117**, 487 (1974).
42. Recent publications, in which earlier references can be found, are: A. R. Sohval, J. P. Delvaille, K. Kalata, K. Kirby-Docken, H. W. Schnopper, *J. Phys. B* **9**, L25 (1976); *ibid.*, p. 47; H. D. Betz, M. Kleber, E. Spindler, F. Bell, H. Panke, W. Stehling, in *The Physics of Electronic and Atomic Collisions*, J. S. Risley and R. Geballe, Eds. (Univ. of Washington Press, Seattle, 1975), p. 520.
43. P. Gippner, *Joint Inst. Nucl. Res. Dubna Publ. No. E-78843* (1975).
44. K. H. Kaun, in *Proceedings of the Second International Conference on Inner-Shell Ionization Phenomena*, W. Mehlhorn, Ed. (University of Freiburg, Freiburg, Germany, in press).
45. K. H. Heinig, H. U. Jäger, H. Richter, H. Woittennek, *Phys. Lett. B* **60**, 249 (1976).
46. W. R. Stott and J. C. Waddington, *Bull. Am. Phys. Soc.* **20**, 638 (1975); R. Anholt and T. K. Saylor, *Lawrence Berkeley Lab. Rep. No. LBL-4066* (1975).
47. W. E. Meyerhof, T. K. Saylor, S. M. Lazarus, A. Little, B. B. Triplett, L. F. Chase, Jr., R. Anholt, unpublished results.
48. W. E. Meyerhof, *Phys. Rev. A* **10**, 1005 (1974).
49. J. S. Greenberg, personal communication.
50. B. Fricke and G. Soff, *Ges. Schwerionenforsch. Rep. No. GSI-T1-74* (1974); B. Fricke, *Ges. Schwerionenforsch. Rep. No. GSI-73-11* (1973), p. 88.
51. G. Bissinger and L. Feldman, *Phys. Rev. A* **8**, 1624 (1973); *Phys. Rev. Lett.* **33**, 1 (1974); J. A. Cairns and L. C. Feldman, in *New Uses of Low Energy Accelerators*, J. F. Ziegler, Ed. (Plenum, New York, in press).
52. R. K. Smith, B. Müller, W. Greiner, J. S. Greenberg, C. K. Davis, *Phys. Rev. Lett.* **34**, 134 (1975). The experimental effect appears to be spurious. See W. Woelfli, C. Stoller, G. Bonani, M. Suter, M. Stoeckli, *ibid.* **35**, 656 (1975).
53. D. Burch, W. B. Ingalls, H. Wieman, R. Vandenbosch, in *Abstracts, 9th International Conference on the Physics of Electronic and Atomic Collisions*, J. S. Risley and R. Geballe, Eds. (Univ. of Washington Press, Seattle, 1975), p. 306; R. Schule, H. Schmidt-Böcking, I. Tserruya, G. Gaukler, K. Bethge, in *ibid.*, p. 304; I. Tserruya, H. Schmidt-Böcking, R. Schule, K. Bethge, R. Schuch, H. J. Specht, *Phys. Rev. Lett.*, in press; F. Jundt, G. Guillaume, P. Fintz, K. U. Jones, *Phys. Rev. A* **13**, 563 (1976).
54. B. Müller, J. Rafelski, W. Greiner, *Phys. Lett. B* **47**, 5 (1973).
55. B. Müller and W. Greiner, *Z. Naturforsch. Teil A* **31**, 1 (1976).
56. S. S. Gershtein and V. S. Popov, *Lett. Nuovo Cimento* **6**, 593 (1973); H. Peitz, B. Müller, J. Rafelski, W. Greiner, *ibid.* **8**, 37 (1973).
57. K. Smith, H. Peitz, B. Müller, W. Greiner, *Phys. Rev. Lett.* **32**, 554 (1974).
58. D. Burch, W. B. Ingalls, H. Wieman, R. Vandenbosch, *Phys. Rev. A* **10**, 1245 (1974).
59. C. Foster, T. Hoogkamer, P. Worlee, F. W. Saris, in *Abstracts, 9th International Conference on the Physics of Electronic and Atomic Collisions*, J. S. Risley and R. Geballe, Eds. (Univ. of Washington Press, Seattle, 1975), p. 511; *J. Phys. B*, in press.
60. J. Rafelski, B. Müller, R. Anholt, personal communications; W. Betz, G. Soff, B. Müller, W. Greiner, in preparation.
61. Systematics established in W. E. Meyerhof, R. Anholt, T. K. Saylor, P. D. Bond [*Phys. Rev. A* **11**, 1083 (1975)] lead to $\sigma_K \approx 3 \times 10^{-25}$ cm^2. From (*18*), $\tau_K = 7 \times 10^{-18}$ sec. For 1600-Mev U, $v_1 = 4 \times 10^9$ cm/sec, and for U, $n = 4.7 \times 10^{22}$ cm^{-3}.
62. V. Oberacker, G. Soff, W. Greiner, *Nucl. Phys. A* **259**, 324 (1976).
63. P. Armbruster, in *Proceedings of the Second International Conference on Inner-Shell Ionization Phenomena*, W. Mehlhorn, Ed. (University of Freiburg, Freiburg, Germany, in press).
64. Enlightening discussions with R. Anholt are gratefully acknowledged. This work was partly supported by the National Science Foundation.

Chromosomal Subunits in Active Genes Have an Altered Conformation

Globin genes are digested by deoxyribonuclease I in red blood cell nuclei but not in fibroblast nuclei.

Harold Weintraub and Mark Groudine

Knowledge of the structure of DNA has provided many insights into its biological function (*1*). In higher cells, a detailed understanding of the structure of chromatin will probably provide analogous insights into how genes are regulated. Already, there are a number of important observations demonstrating a relation between the structure of chromatin and its biological activity (*2*, *3*).

The packaging of most of the nuclear DNA is now thought to be based on repeating units of about 180 to 200 base pairs of DNA associated with specific complexes of histones (*4*, *5*), possibly two self-complementary tetramers each containing one of the four major histones (*6*). These two tetramers could define the twofold axis of symmetry within the nucleosome. These complexes interact through 70 to 90 amino acid residues at their carboxyl terminal end to produce a tight, trypsin-resistant core (*7*). The positively charged histone amino terminal residues extend outward from this core and define what may prove to be a "kinked" or "coiled" pathway for the DNA (*5*, *8*) about the histone complexes. These so-called "particles-on-a-string" or "nu" bodies constitute the primary level of folding for the bulk of the chromosome. Through their mutual interactions higher levels of DNA packaging can be achieved, although details of this organization are not known. At present there is no proof that nu bodies are homo-

Dr. Weintraub is an assistant professor in the Department of Biochemical Sciences, Frick Laboratories, Princeton University, Princeton, New Jersey 08540. Dr. Groudine was a visiting fellow in the same department and is now at the Department of Radiation Oncology, University of Washington Hospital, Seattle 98105.